Journal of Solid State Chemistry **156,** 32–36 (2001)
doi:10.1006/jssc.2000.8954, available online at http://www.idealibrary.com on IDEAL®

The Synthesis and Characterization of a New Manganese Phosphate Templated by Piperazine

Kjell Ove Kongshaug, Helmer Fjellvåg, and Karl Petter Lillerud

Department of Chemistry, University of Oslo, P.O Box 1033 Blindern, N-0315 Oslo, Norway

Received May 23, 2000; in revised form August 1, 2000; accepted September 5, 2000; published online December 21, 2000

An organically templated manganese phosphate, $Mn_6(H_2O)_2(HPO_4)_4(PO4)_2 \cdot C_4N_2H_{12} \cdot H_2O$, has been synthesized hydrothermally and characterized by synchrotron powder X-ray diffraction, thermogravimetric analysis, and magnetic measurements. The compound is structurally closely related to both a magnesium phosphate and an iron phosphate, and crystallizes in the triclinic space group *P*-1 (No. 2) with $a = 12.81926(12)$ Å, $b = 15.87361(20)$ Å, $c = 6.47912(7)$ Å, $\alpha = 99.8660(11)^\circ$, $\beta = 90.3913(10)^\circ$, $\gamma = 103.4265(9)^\circ$, $V = 1261.928(25)$ Å^3, and $Z = 2$. The structure consists of anionic sheets of manganese phosphate separated by piperazinium cations and water molecules. The basic building unit of the inorganic layers is a hexamer of edge-sharing Mn polyhedra. Magnetic susceptibility measurements and bond valence calculations confirm the assignment of high-spin Mn^{2+} (d^5) in the title compound.

INTRODUCTION

Currently there is considerable research interest in the use of organic templates to direct the synthesis of micro- and mesoporous materials (1, 2). This activity stems from the possible application of such materials as molecular sieves, sorbents, and catalysts. Most of these organic–inorganic hybrid materials contain silicon, aluminum, and phosphorus, but also transition metals have successfully been incorporated into layered and three-dimensional frameworks. Such materials include phosphates of molybdenum (3), vanadium (4), iron (5), cobalt (6), zirconium (7), and titanium (8). The transition metal-containing materials may have new and exciting applications, for instance, as redox catalysts.

Until now just one organic–inorganic hybrid material based on manganese phosphate has been known to exist (9). In addition a number of organically templated three-dimensional manganese–gallium phosphates have been known (10–12). Manganese phosphates are also found in nature as minerals like switzerite (13). In addition a number of synthetic phosphates have been obtained. The compounds contain structure elements of chains (14) or layers (15) or exhibit a dense three-dimensional network (16). When it comes to oxidation state, compounds containing either Mn^{II} (17) or Mn^{III} (18) have been known as well as mixed-valence Mn^{II}/Mn^{III} compounds (19). In addition, manganese itself has been known to form microporous and layered oxide structures (20). These materials exhibit mixed valence and manganese oxidation state in the range 3.5–3.8.

Presently, the synthesis and crystal structure of an organically templated layered manganese phosphate, UiO-23, is reported. The compound was synthesized hydrothermally, and the crystal structure was solved from high-resolution synchrotron powder X-ray diffraction data. The thermal and magnetic behavior of the compound has been studied.

EXPERIMENTAL

Synthesis

UiO-23 was synthesized hydrothermally from a mixture of manganese acetate tetra hydrate (Aldrich, 99%), phosphoric acid (Merck, 85%), piperazine hexahydrate (Fluka, 98%) deionized water in a molar ratio of 2:3:2:50. This mixture had an initial pH of 3.8. The crystallization took place in a Teflon-lined steel autoclave, filled to 80% of maximum volume, at 150°C for four days. The final pH after crystallization was 3.6. The product in form of a white powder was washed with water and dried in air at 60°C. The yield based on Mn was 50%.

Crystal Structure Determination

Synchrotron powder X-ray data were collected at the Swiss–Norwegian Beam Line (BM1) at ESRF, Grenoble. The data were collected in transmission mode in a 1.0-mm rotating capillary ($\lambda = 0.52227$ Å; 2θ range 1.6°–2.1° and 4.38°–25.272°, which resulted in 5348 observations and 1608 contributing reflections). The powder pattern was indexed in a triclinic unit cell using the autoindexing program ITO (21): $a = 12.81926(12)$ Å, $b = 15.87361(20)$ Å,

0022-4596/01 $35.00

TABLE 1
Experimental Conditions and Relevant Data for the Rietveld Refinements of UiO-23

Chemical formula	$Mn_6(H_2O)_2(HPO)_4(PO4)_2 \cdot C_4N_2H_{12} \cdot H_2O$
Formula weight	1045.696
Pattern range 2θ (°)	1.6–2.1 and 4.38–25.272
Step size $\Delta 2\theta$ (°)	0.004
Wavelength (Å)	0.52227
Space group	*P*-1 (No. 2)
a (Å)	12.81926(12)
b (Å)	15.87361(20)
c (Å)	6.47912(7)
α (°)	99.8660(11)
β (°)	93.260(2)
χ (°)	103.4265(9)
Z	2
V (Å^3)	1261.928(25)
No. of observations	5348
No. of reflections	1608
No. of refined parameters	177
R_{wp}	0.083
R_F^2	0.071

$c = 6.47912(7)$ Å, $\alpha = 99.8660(11)^\circ$, $\beta = 90.3913(10)^\circ$, $\gamma = 103.4265(9)^\circ$, and $V = 1261.928(25)$ Å^3. A starting model for Rietveld refinement in space group *P*-1 (no. 2) was built on the basis of the structurally related magnesium phosphate UiO-16 (22) using the Cerius^2 software. The refinement was carried out using GSAS (23). Initially, scale, background, zero point, and lattice parameters were refined. The profile parameters were optimized by fitting the pattern using the LeBail method (24). Atomic positions were refined with soft constraints being introduced: d(P–O) = 1.54(2), d(Mn–O) = 2.15(5), d(N–C) = 1.48(2) and d(C–C) = 1.52(2) Å. The weight function could not be completely lifted at the end of the refinement without unrealistic bond distances emerging in the structure. Common isotropic displacement parameters were adopted for manganese, phosphorous, framework oxygen atoms and template nitrogen and carbon atoms, respectively. The final residuals were $R_{wp} = 0.083$ and $R_F^2 = 0.071$ refined with 177 parameters. The largest peak and hole in the Fourier difference map are 0.671 and -0.551 eÅ^{-3}. Experimental conditions of the Rietveld refinement are reported in Table 1. Atomic coordinates and isotropic displacement parameters are given in Table 2 and selected bond distances are presented in Table 3. Figure 1 shows the observed, calculated and difference diffraction profiles from the Rietveld analysis.

Thermogravimetric Analysis

Thermogravimetric analysis (TGA) was carried out in a flow of nitrogen on a Scientific Rheometric STA 1500. The sample (20 mg) was heated from room temperature to 800°C at a rate of 5 K min^{-1}.

Magnetic Measurements

The magnetization of the compound was measured in a field of 1000 G over the temperature ranges 5–305 K with a step of 10 K and 2–20 K with a step of 1 K. The experiments were performed on a Quantum Design MPMS SQUID magnetometer.

TABLE 2
Atomic Coordinates and Isotropic Displacement Parameters for UiO-23

Atom	*x*	*y*	*z*	U_{iso} (Å^2)
P1	0.6544(9)	0.0121(8)	0.6526(17)	0.0233(19)
P2	0.8467(9)	0.9900(8)	0.1463(17)	0.0233(19)
P3	0.4711(10)	0.8088(9)	0.8470(18)	0.0233(19)
P4	0.0291(10)	0.1909(9)	0.5082(20)	0.0233(19)
P5	0.7121(11)	0.3463(10)	0.6809(21)	0.0233(19)
P6	0.7899(10)	0.6478(10)	0.8748(19)	0.0233(19)
Mn1	0.5894(6)	0.9980(6)	0.1599(11)	0.0125(11)
Mn2	0.9098(6)	0.0042(6)	0.6594(10)	0.0125(11)
Mn3	0.7671(6)	0.1701(5)	0.3814(10)	0.0125(11)
Mn4	0.7326(6)	0.8306(5)	0.7358(10)	0.0125(11)
Mn5	0.5155(6)	0.8240(5)	0.3793(10)	0.0125(11)
Mn6	0.9842(6)	0.1786(5)	0.0315(11)	0.0125(11)
O1	0.7414(11)	0.9630(11)	0.689(4)	0.0168(18)
O2	0.6977(19)	0.1105(10)	0.6393(28)	0.0168(18)
O3	0.5810(17)	0.9635(10)	0.4602(20)	0.0168(18)
O4	0.5791(12)	0.0033(19)	0.8331(22)	0.0168(18)
O5	0.8050(18)	0.8917(10)	0.0464(26)	0.0168(18)
O6	0.7599(10)	0.0403(10)	0.2120(32)	0.0168(18)
O7	0.9178(15)	0.0382(10)	0.9943(22)	0.0168(18)
O8	0.9221(11)	0.9997(19)	0.3380(20)	0.0168(18)
O9	0.4158(19)	0.7132(11)	0.866(4)	0.0168(18)
O10	0.5571(11)	0.7972(17)	0.6857(21)	0.0168(18)
O11	0.3935(12)	0.8574(10)	0.7627(33)	0.0168(18)
O12	0.5191(18)	0.8534(10)	0.0693(20)	0.0168(18)
O13	0.0967(18)	0.2810(12)	0.6230(34)	0.0168(18)
O14	0.9425(11)	0.2050(17)	0.3595(22)	0.0168(18)
O15	0.1056(12)	0.1413(10)	0.3839(31)	0.0168(18)
O16	0.9743(17)	0.1493(10)	0.6897(21)	0.0168(18)
O17	0.6985(20)	0.4257(13)	0.5840(34)	0.0168(18)
O18	0.7771(17)	0.3614(18)	0.8918(28)	0.0168(18)
O19	0.7858(16)	0.2969(11)	0.5509(33)	0.0168(18)
O20	0.5957(14)	0.2954(13)	0.692(4)	0.0168(18)
O21	0.8078(21)	0.5733(14)	0.7014(30)	0.0168(18)
O22	0.7242(17)	0.6212(18)	0.0637(29)	0.0168(18)
O23	0.7204(17)	0.6979(11)	0.7706(33)	0.0168(18)
O24	0.8943(14)	0.7098(13)	0.9779(35)	0.0168(18)
OW1	0.6834(13)	0.8037(18)	0.3275(34)	0.014(10)
OW2	0.8214(14)	0.2089(18)	−0.020(4)	0.009(10)
OW3	0.7162(31)	0.4634(29)	0.138(5)	0.189(21)
N1	0.9967(23)	0.4073(19)	0.472(5)	0.005(6)
N2	0.5176(23)	0.5913(20)	0.571(5)	0.005(6)
C1	0.9351(23)	0.4382(24)	0.317(5)	0.005(6)
C2	0.9954(27)	0.5335(24)	0.323(4)	0.005(6)
C3	0.5683(24)	0.5633(25)	0.375(5)	0.005(6)
C4	0.5088(28)	0.4699(25)	0.278(5)	0.005(6)

Note. Calculated standard deviations are in parentheses. Space group is *P*-1.

TABLE 3
Selected Bond Distances (Å) for UiO-23

P1–O1	1.539(6)	Mn1–O3	2.107(13)
P1–O2	1.550(6)	Mn1–O4	2.117(12)
P1–O3	1.534(6)	Mn1–O4	2.182(13)
P1–O4	1.537(6)	Mn1–O6	2.138(13)
		Mn1–O11	2.222(13)
		Mn1–O12	2.236(13)
P2–O5	1.548(6)	Mn2–O1	2.126(13)
P2–O6	1.536(6)	Mn2–O7	2.140(13)
P2–O7	1.528(6)	Mn2–O8	2.080(12)
P2–O8	1.533(6)	Mn2–O8	2.170(13)
		Mn2–O15	2.240(12)
		Mn2–O16	2.233(13)
P3–O9	1.545(6)	Mn3–O2	2.156(13)
P3–O10	1.544(6)	Mn3–O6	2.143(12)
P3–O11	1.542(6)	Mn3–O11	2.172(12)
P3–O12	1.547(6)	Mn3–O14	2.199(13)
		Mn3–O19	2.081(13)
		Mn3–OW2	2.703(12)
P4–O13	1.549(6)	Mn4–O1	2.151(12)
P4–O14	1.543(6)	Mn4–O5	2.177(12)
P4–O15	1.544(6)	Mn4–O10	2.197(12)
P4–O16	1.541(6)	Mn4–O15	2.193(12)
		Mn4–O23	2.127(13)
		Mn4–OW1	2.653(12)
P5–O17	1.543(6)	Mn5–O3	2.149(13)
P5–O18	1.549(6)	Mn5–O10	2.187(13)
P5–O19	1.532(6)	Mn5–O12	2.137(12)
P5–O20	1.531(6)	Mn5–O20	2.068(13)
		Mn5–OW1	2.269(13)
P6–O21	1.544(6)	Mn6–O7	2.163(13)
P6–O22	1.552(6)	Mn6–O14	2.189(13)
P6–O23	1.545(6)	Mn6–O16	2.180(12)
P6–O24	1.535(6)	Mn6–O24	2.080(12)
		Mn6–OW2	2.281(13)
N1 C1	1.483(6)	N2 C4	1.479(6)
N1 C2	1.482(6)	C1 C2	1.525(6)
N2 C3	1.481(6)	C3 C4	1.523(6)

Note. Calculated standard deviations are in parentheses.

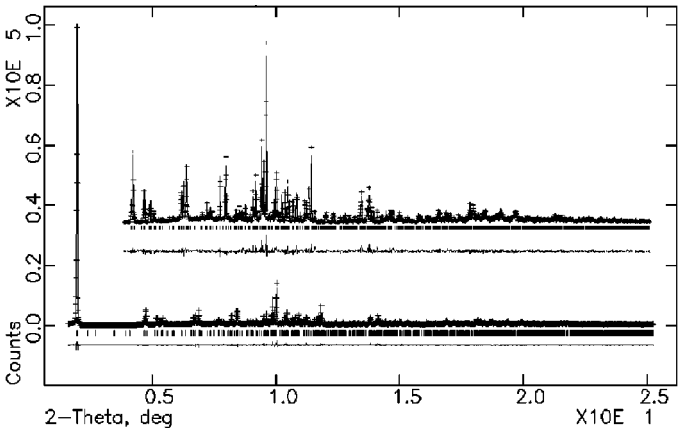

FIG. 1. Final diffraction profiles from Rietveld refinement of synchrotron radiation data.

RESULT AND DISCUSSION

Thermogravimetric Analysis

Thermogravimetric analysis shows a total weight loss of 12.8% in two steps below 400°C (Fig. 2). This is in agreement with first the loss of three water molecules and thereafter loss of the organic template (calculated loss 13.6%). Above 400°C the structure collapses, and the resulting X-ray powder diffraction pattern indicates an amorphous state.

Crystal Structure

The crystal structure of UiO-23, $Mn_6(H_2O)_2(HPO)_4(PO4)_2 \cdot C_4N_2H_{12} \cdot H_2O$, contains inorganic layers of anionic manganese phosphate connected by interlamellar piperazinium cations and water molecules (Fig. 3). UiO-23 is structurally closely related to both a magnesium phosphate (22) and an iron phosphate (25), and is a triclinic variant of these two monoclinic compounds containing the same structural features. UiO-23 has 45 nonhydrogen atoms in the asymmetric unit (6 Mn, 6 P, 27 O, 2 N, and 4 C), and is among the more complex structures being refined from powder diffraction data. The basic building unit in the manganese phosphate layers is a hexamer composed of two MnO_6 octahedra, two $MnO_5(H_2O)$ octahedra, and two $MnO_4(H_2O)$ tetragonal pyramids (Fig. 4). All these polyhedra are connected via edge sharing. The hexamers have two orientations within the layers (Fig. 5), and are interconnected via manganese polyhedra and via phosphate tetrahedra. A bond valence analysis (26) indicates presence of just divalent manganese consistent with the results of the magnetic measurements. The six crystallographically

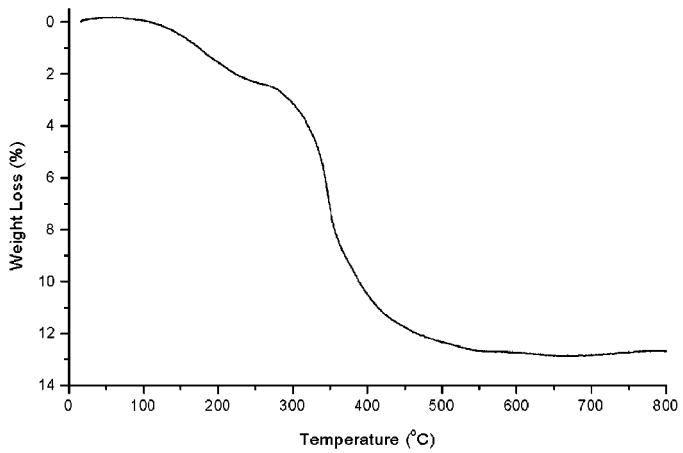

FIG. 2. TG curve for UiO-23 heated at a rate of $5\ K \cdot min^{-1}$.

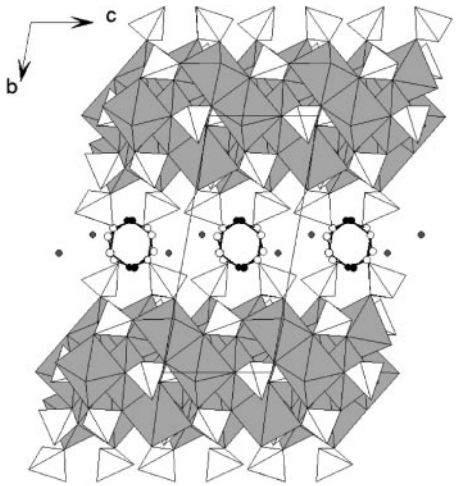

FIG. 3. View along [100] of the crystal structure of UiO-23 showing anionic manganese phosphate layers as coordination polyhedra and pipirazinium cations and water molecules in the interlamellar space.

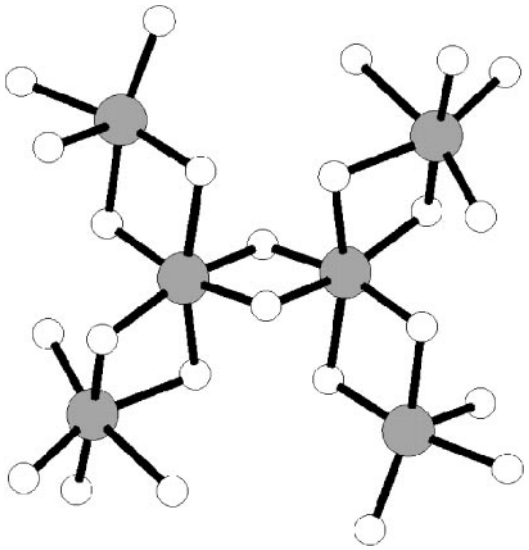

FIG. 4. The basic building unit of the manganese phosphate layers in the form of a hexamer of edge-sharing manganese polyhedra.

independent phosphate tetrahedra can also be grouped in three pairs of two. In two tetrahedra all the four oxygen atoms are bridging to manganese polyhedra. Two tetrahedra have three bridging and one terminal oxygen, the latter most probably being an OH group due to a hydrogen bonding contact to a bridging oxygen ($d(\mathrm{O9}\cdots\mathrm{O20}) = 2.89$ and $d(\mathrm{O13}\cdots\mathrm{O24}) = 2.57$ Å). The last two phosphate tetrahedra are composed of two bridging and two terminal oxygen atoms. Two of them are OH groups, whereas the nature of the last two is more uncertain. For these, there is hydrogen bonding contacts to the nitrogen atoms of the piperazine molecules. However, the powder X-ray data do not allow determination of hydrogen positions. It is possible that the piperazine molecules are doubly protonated, however, the terminal oxygen atoms might be OH groups or there may exist disorder in the hydrogen positions as was found for UiO-16 (22). The formula given for UiO-23 assumes that the piperazine molecules are doubly protonated.

The synthesis of UiO-23 represents one of the first examples of a organic–inorganic hybrid material based on manganese phosphate. Both UiO-23 and the other phase, $(C_2H_{10}N_2)[Mn_2(HPO_4)_3(H_2O)]$ (9), reported so far have been of layered nature. The next step in the development would be to synthesize organically templated manganese phosphates with 3D open framework structures just as we have managed in the magnesium phosphate system with UiO-20 (27).

Magnetic Properties

The temperature dependence of the molar magnetic susceptibility showed Curie–Weiss behavior in the range 15–305 K (Fig. 6). The measured points were fitted with $\chi_m = C_m/(T - \theta)$, where C_m and θ are the Curie and Weiss constants, respectively. The observed Curie constant of $C_m = 4.19\ \mathrm{emu}\cdot\mathrm{K}^{-1}\cdot\mathrm{mole}^{-1}$ corresponds to an effective paramagnetic moment of $\mu_{\mathrm{eff}} = 5.79\cdot\mu_B$, which is close to the spin-only value of $5.92\cdot\mu_B$ for Mn^{II} (d_5). The deviation in μ_{eff} may be caused by spin–orbit coupling of Mn^{II} in the distorted five- and six coordinated environments.

The Weiss constant of -36.22 K indicates rather weak antiferromagnetic interactions between the Mn^{II} atoms. At low temperatures, the magnetic susceptibility increases strongly below 7 K, see inset to Fig. 6, which indicates onset of long-range antiferromagnetic order. For the layered $(C_2H_{10}N_2)[Mn_2(HPO_4)_3(H_2O)]$ a maximum in $\chi_m(T)$ occurs around 2.5 K (9). For the latter, the crystal structure

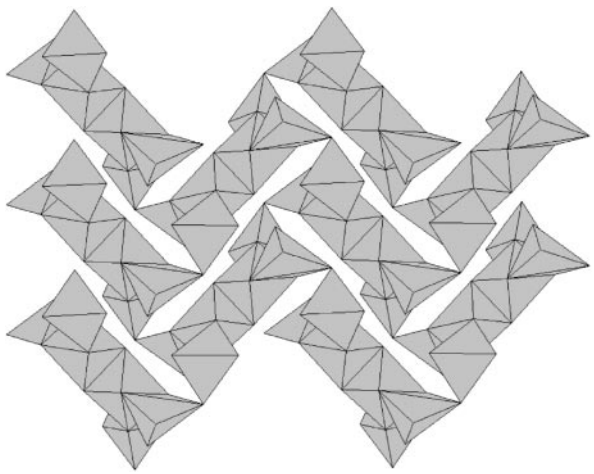

FIG. 5. The interconnection of Mn polyhedra forming the 2D layers.

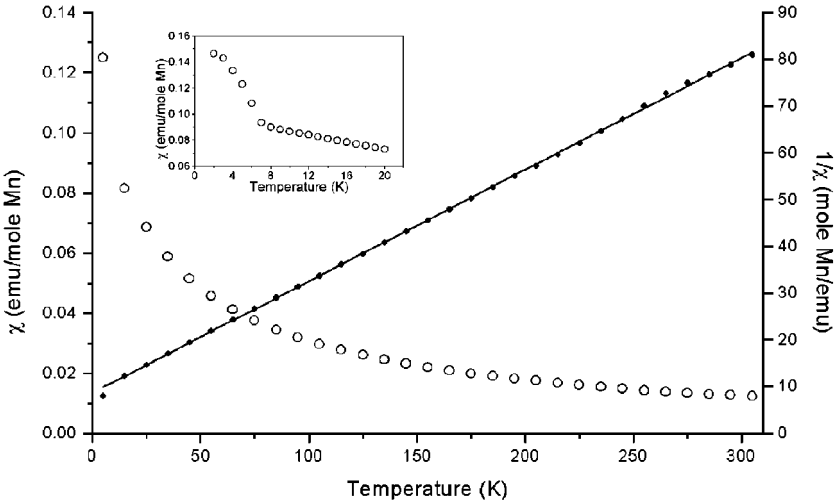

FIG. 6. Magnetic susceptibility and reciprocal susceptibility as a function of temperature for UiO-23.

contains zig-zag chains with a Mn_3O_{13} cluster formed by edge-sharing octahedra and a bridging MnO_5 trigonal bipyramid. On that basis the susceptibility was described using a triangular lattice antiferromagnetic model with $S = 5/2$ (9). The interlayer Mn–Mn separation is comparable to that in UiO-23 (around 10 Å). However, in UiO-23 the magnetic sublattice contains interconnected hexameric units (Fig. 5) of Mn polyhedra, which probably explains the substantially increased ordering temperature.

ACKNOWLEDGMENT

The skillful assistance from the project team at the Swiss–Norwegian Beam Line, ESRF is gratefully acknowledged.

REFERENCES

1. A. K. Cheetham, G. Ferey, and T. Loiseau, *Angew. Chem. Int. Ed. Engl.* **38,** 3268 (1999).
2. J. Y. Jing, C. P. Mehnert, and M. S. Wong, *Angew. Chem. Int. Ed. Engl.* **38,** 56 (1999).
3. R. C. Haushalter, K. G. Strohmaier, and F. W. Lai, *Science* **246,** 1289 (1989).
4. V. Soghomonian, Q. Chen, R. C. Haushalter, J. Zubieta, and C. J. O'Connor, *Science* **259,** 1596 (1993).
5. M. Cavellec, D. Riou, and G. Ferey, *J. Solid State Chem.* **112,** 441 (1994).
6. J. Chen, R. H. Jones, S. Natarajan, M. B. Hursthouse, and J. M. Thomas, *Angew. Chem. Int. Ed. Engl.* **33,** 639 (1994).
7. E. Kemnitz, M. Wloka, S. Trojanov, and A. Stiewe, *Angew. Chem. Int. Ed. Engl.* **35,** 2677 (1996).
8. D. M. Poojary, A. I. Bortun, L. N. Bortun, and A. Clearfield, *J. Solid State Chem.* **132,** 213 (1997).
9. J. Escobal, J. L. Pizarro, J. L. Mesa, L. Lezama, R. Olazuaga, M. I. Arriortua, and T. Rojo, *Chem. Mater.* **12,** 376 (2000).
10. A. D. Bond, A. M. Chippindale, A. R. Cowley, and A. V. Powell, *Zeolites* **19,** 326 **(**1997).
11. A. M. Chippindale, A. D. Bond, A. R. Cowley, and A. V. Powell, *Chem. Mater.* **9,** 2830 (1997).
12. A. M. Chippindale and A. R. Cowley, *Microporous Mesoporous Mater.* **21,** 271 (1998).
13. P. F. Zanazzi, P. B. Leavens, and J. S. White, *Am. Miner.* **71,** 1224 (1986).
14. L. Fanfani, A. Nunzi, and P. F. Zanazzi, *Acta Crystallogr. Sect. B* **26,** 640 (1970).
15. Y. Cudennec, A. Riou, and Y. Gerault, *Acta Crystallogr. Sect. C* **41,** 1411 (1989).
16. F. Leroux, A. Mar, D. Guyomard, and Y. Piffard, *J. Solid State Chem.* **117,** 206 (1995).
17. F. A. Ruszala, J. B. Anderson, and E. Kostiner, *Inorg. Chem.* **16,** 2417 (1977).
18. P. Lightfoot and A. K. Cheetham, *J. Solid State Chem.* **78,** 17 (1989).
19. A. R. Kampf and P. B. Moore, *Am. Miner.* **61,** 1241 (1976).
20. S. T. Suib, *Curr. Opin. Solid State Mater. Sci.* **3,** 63 (1998).
21. J. W. Visser, *J. Applied Crystallogr.* **2,** 89 (1969).
22. K. O. Kongshaug, H. Fjellvåg, and K.P. Lillerud, *Chem. Mater.* **11,** 2872 (1999).
23. A. C. Larson and R. B. von Dreele, Los Alamos Natl. Lab. Rep. LA-UR-86-784 (1987).
24. A. Le Bail, H. Duroy, and J. Fourquet, *Mater. Res. Bull.* **23,** 447 (1988).
25. V. Zima, K. W. Lii, N. Nguyen, and A. Ducouret, *Chem. Mater.* **10,** 1914 (1998).
26. N. E. Brese and M. O'Keeffe, *Acta Crystallogr. Sect. B* **47,** 192 (1991).
27. K. O. Kongshaug, H. Fjellvåg, and K. P. Lillerud, *Chem. Mater.* **12,** 1095 (2000).